INSTITUT D'AERONOMIE SPATIALE DE BELGIQUE

3 - Avenue Circulaire
B - 1180 BRUXELLES

AERONOMICA ACTA

A - N° 235 - 1981

Stratospheric aerosols properties from earth limb photography and Mie scattering theory

by

M. ACKERMAN, C. LIPPENS and C. MULLER

BELGISCH INSTITUUT VOOR RUIMTE-AERONOMIE

3 - Ringlaan
B - 1180 BRUSSEL

FORWORD

A more concise version of the text presented here is published as an article in Nature under the title : "Stratospheric aerosol properties from the earth limb photography" (Nature, 292, 587-591 (1981)).

AVANT-PROPOS

Une version plus concise du texte présenté ici est publié comme article dans Nature sous le titre : "Stratospheric aerosol properties from earth limb photography" (Nature, 292, 587-591 (1981)).

VOORWOORD

Een verkorte versie van deze tekst wordt als artikel gepubliceerd in Nature onder de titel : "Stratospheric aerosol properties from earth limb photography" (Nature, 292, 587-591 (1981)).

VORWORT

Eine kurzgefasster Version dieser Text ist in der Zeitschrift "Nature" unter dem Titel : "Stratospheric aerosol properties from earth limb photography" (Nature, 292, 587-591 (1981)).

STRATOSPHERIC AEROSOLS PROPERTIES FROM EARTH LIMB PHOTOGRAPHY AND MIE SCATTERING THEORY

by

M. ACKERMAN, C. LIPPENS and C. MULLER

Abstract

The balloon borne observation at three wavelengths of visible sunlight scattered by the earth limb allows the determination of aerosols abundances and size distributions versus altitude in the stratosphere. The stratospheric aerosols appear to still remain under the influence of the Mount St. Helens volcanic eruption five months after its occurence on May 18, 1980.

It is shown that the method is, in the stratospheric conditions sensitive to particles in the size range from 0.04 μm to 0.4 μm radius. A comparison with previous data allows to state that the number of particles smaller than 0.1 μm radius has up to now been underestimated. This conclusion stems from the relatively low asymmetry factors observed for the scattering phase functions which are important for radiative transfer and earth energy budget evaluations.

Résumé

L'observation, à partir d'une nacelle de ballon stratosphérique et à trois longueurs d'onde, de la diffusion du rayonnement solaire visible permet la détermination de l'abondance et des distributions de taille de l'aérosol stratosphérique en fonction de l'altitude. L'aérosol stratosphérique est encore sous l'influence de l'éruption volcanique du Mont St. Helens cinq mois après qu'elle ait eu lieu le 18 mai 1980.

On montre que la méthode est, dans les conditions stratosphériques, sensible aux particules de rayon compris entre 0,04 µm et 0,4 µm. Une comparaison avec les données antérieures permet d'affirmer que le nombre de particules de rayon inférieur à 0,1 µm a été sous estimé jusqu'ici. Cette conclusion résulte des valeurs relativement faibles observées pour le facteur d'asymétrie des fonctions de phase qui sont importantes pour l'évaluation du transfert radiatif et du budget énergétique de la terre.

Samenvatting

De waarneming, op drie golflengten van het verstrooide zichtbare zonlicht nabij de aardse kim vanaf een gondel aan een stratosfeerballon, laat toe de dichtheids en afmetingen distributie van de stratosferische aerosols te bepalen in functie van de hoogte.

Vijf maanden na de eruptie van de Mount St. Helens vulkaan op 18 mei 1980, is de invloed ervan op de stratosferische aerosols nog steeds merkbaar. Er wordt aangetoond at de methode, onder stratosferische voorwaarden, gevoelig is voor deeltjes waarvan de straal begrepen is tussen 0,04 µm en 0,4 µm.

Een vergelijking met vroegere gegevens leidt ons tot de vaststelling dat het aantal deeltjes waarvan de straal kleiner is dan 0,1 µm tot hiertoe onderschat werd. Dit besluit volgt uit de relatief lage assymetriefactor waargenomen voor de verstrooiïngsfasefunctue, die belangrijk is voor de berekening van de stralingsoverdracht en het energie budget van de aarde.

Zusammenfassung

Die Ballonenbeobachtungen auf drei Wellenlänge der sichtbaren zerstreuten Sonnenstrahlung erlauben eine Bestimmung der stratosphärischen Aerosolzahl und der Aerosolgrösse. Die stratosphärischen Aerosolen sind fünf Monaten nach der Mount St. Helen Vulkaneruption auf den 18.Mai 1980 noch dadurch beeinflusst.

Unter stratosphärischen Zuständen ist die Methode für Aerosolgrössen zwischen 0,04 µm und 0,4 µm empfindlich. Eine Vergleichung mit vorherigen Daten zeigt, dass die Aerosolzahl mit Halbnesser kleiner als 0,1 µm bis jetz unterabgeschätzt ist. Dieser Abschluss ergibt sich aus der ziemlich kleine beobachtete asymetrische Faktoren der Phasefunktion, die wichtig sind für Strahlungsübertragungs- und Energiebilanz- Rechnungen.

INTRODUCTION

The various light phenomena in the atmosphere like the varying blue of the sky, the rosy dawn, etc. to which aerosols may participate belong to the number of ancient sciences whose origines are lost in prehistoric times[1]. It is however only relatively recently that dedicated studies of the stratospheric aerosols were initiated to understand the properties of these particles which are of definite concern as nucleating and catalytic agents and important consituents in determining the radiation balance of the atmosphere. A survey of light scattering techniques used in the remote monitoring of atmospheric aerosols has been published recently[2]. Twilight phenomena have been used both from the ground[3,4] and from satellites. Earth limb observation from space has been based on sunlight scattering observed directly[5,6] or through its absorption[7]. In situ sampling initiated twenty years ago[8] has also provided much information particularly about the composition as recently reviewed[9].

We already reported[10] on the photographic observation, from a balloon gondola floating in the upper stratosphere, of the enhancement of stratospheric aerosols over Europe 23 days after the Mount St. Helens volcanic eruption. Several other reports have now appeared[11,12,13,14] on the subject while details have been provided on the air trajectories which have lead the volcanic plume to move at various altitudes in various directions[15] at the beginning of their many cumbersome revolutions around the earth. Much information has been collected on the properties of the ejecta in relation with atmospheric effects[16]. On October 15, 1980, five months after the eruption an other photographic balloon flight was performed. One of the first results is that the enhancement of stratospheric aerosols below 20 km altitude has become very horizontally homogeneous. This situation allows to take easily advantage of most of the method's potentialities to determine basic properties of volcanically influenced aerosols and of

natural aerosols wich appear to differ in several respects in the stratosphere.

PRINCIPLES OF THE OBSERVATION METHOD

Photographic cameras on board of a balloon gondola simultaneously record at various wavelengths the light from the earth limb below the horizontal line of sight while the solar elevation is low. This light is scattered direct sunlight with a contribution from the earth albedo which is minimized when the sun is low. The observation geometry is shown in figure 1. The limb radiance, R, can be expressed directly in solar radiance units since solar images are recorded simultaneously with a known attenuation factor. The solar elevation is known from the time of picture taking and from the geographic position. From several consecutive shots an angular scale is constructed. The depression angles at which radiances are measured are related to the line of sight altitude of closest approach to the earth surface taking into account the refraction effects[17]. The measured integrated radiances can be inverted taking into account absorption by ozone and air along the line of sight by the "onion pealing" method to yield the in situ radiance, R^*, per unit length versus altitude.

The sun oriented gondola can be rotated about its vertical axis in order that pictures are taken at various azimuth angles, A, relative to the sun position as shown in figure 2. The scattering angle θ of direct solar radiation can be computed from the relation

$$\cos \theta = - \sin D \sin h_{\odot} + \cos D \cos h_{\odot} \cos A \qquad (1)$$

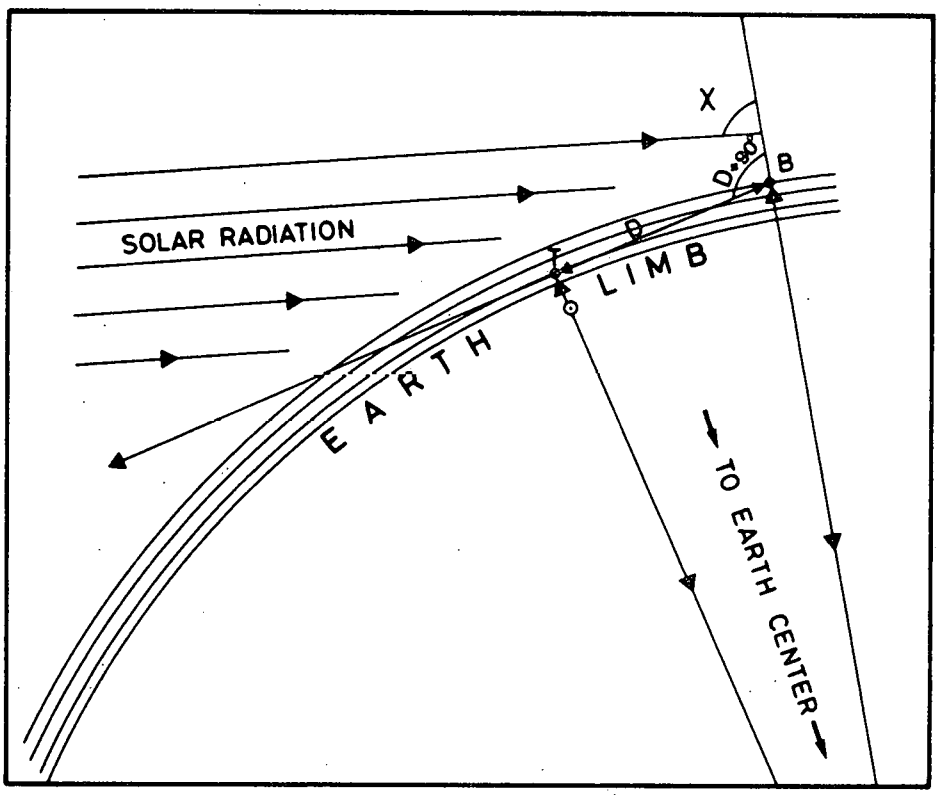

Fig. 1.- Observationnal geometry : quasi parallel light falls on the atmosphere at a solar zenith angle χ, the atmosphere is seen at various depression angles D; through the rotation of the gondola, photographs are taken at various azimuth angles from the sun direction.

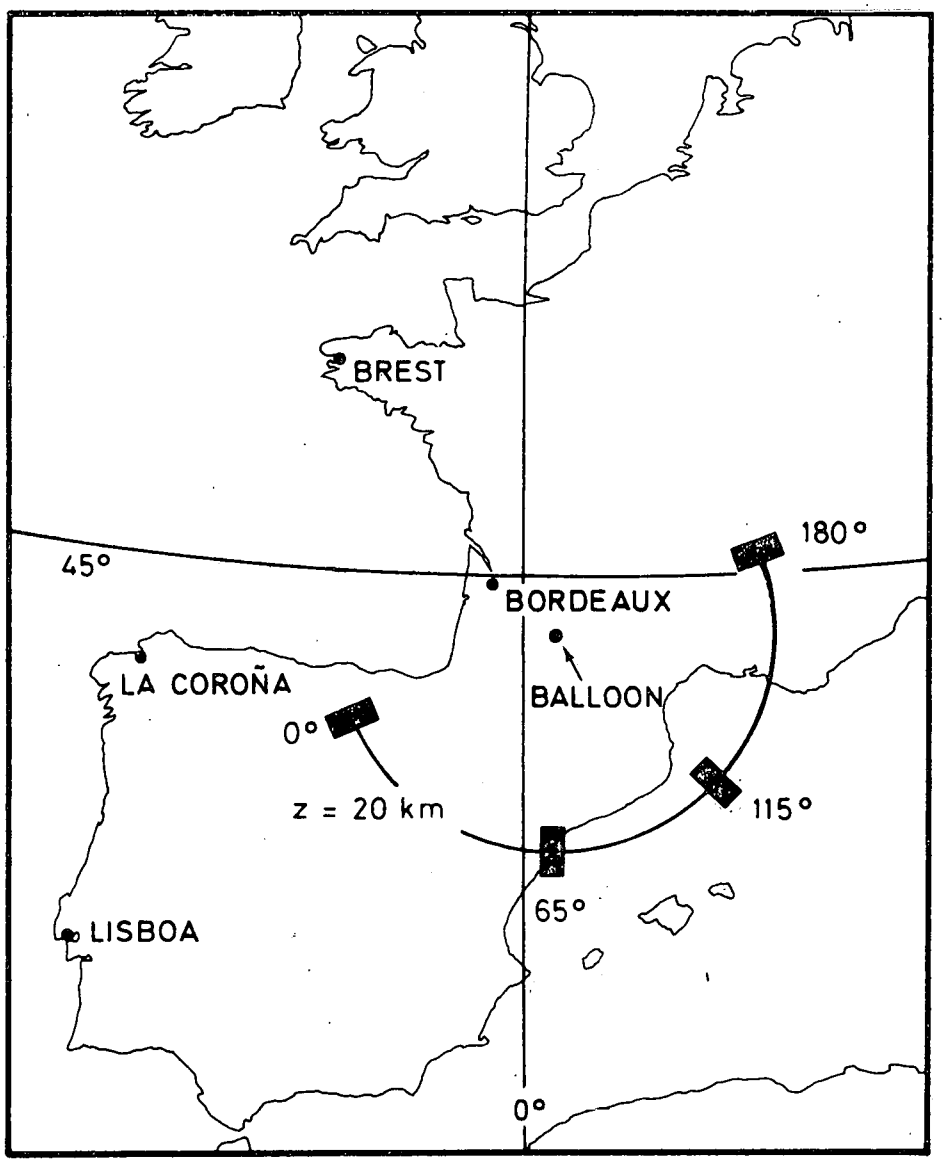

Fig. 2.- Map showing the geographical extent of the measurements. The half circle shows the positions of the tangent points of the line of sight at 20 km altitude. The sun azimuth is at 0°.

where D is the depression angle at which the atmospheric radiance is measured and $h_\odot$ is the solar elevation angle at the time of measurement. As expected from their strong forward scattering properties, and as observed, aerosols reemit little light at an azimuth angle 180 degree away from the sun direction. The limb radiance observed in this case is used to subtract Rayleigh scattering and isolate aerosols scattering at all azimuths taking into account the Rayleigh phase function[18].

If only direct solar radiation is considered an in situ monodisperse aerosol radiance R_a^* per cm of path length is related to the average solar radiance $R_\odot$ by

$$R_a^* = R_\odot \pi \alpha^2 Q_s \sigma \varphi_\theta n/4\pi \qquad (2)$$

where α, φ_θ, Q_s and σ_θ are respectively the angular radius of the sun's disk, 4.65×10^{-3} radian, the properly normalized particulate phase function, the scattering efficiency factor, the particulate scattering geometrical cross section in cm^2 if the number density, n, of the particles is expressed in cm^{-3}.

In practice, our data confirm the previous observation[19] according to which the phase function can, within experimental uncertainties, be represented by the Henyey-Greenstein function. The asymmetry factor g of the phase function can then be determined as well as the total scattering efficiency. The variation of these parameters with wavelength can be fitted to their theoretical variations with the effective size parameter as shown by Hansen and Travis[20]. This procedure, which has been performed using the Mie scattering computation programme provided by Wiscombe[21], leads to an evaluation of the effective particle size and provides information on other

properties too. From these two quantities and from the product $n\sigma$ obtained directly from the relation 2 the value of n can be deduced.

A few terms[20] will be recalled here as they will be used in the interpretation of the data. The aerosol particle size is usually treated in terms of the wavelength, λ, of the interacting light through the Mie size parameter

$$x = 2 \pi a/\lambda \tag{3}$$

where a is the radius of the spherical particle in a monodisperse aerosol. In a polydisperse aerosol the number of particles of radius r is expressed[20] by

$$n_r = A\, r^{(1 - 3b)/b}\, \ell^{-r/ab} \tag{4}$$

where a becomes the effective radius while b is a measure of the width of the size distribution; A is a constant related to the total number of particles.

The measurement of R_a^* versus θ, the scattering angle, at various wavelengths provides information about the asymmetry factor, g. The knowledge of g and its variation with the wavelength of the interacting light leads to the unique determination of a and b as shown in figure 3. The scattering efficiency Q_s can then be determined versus size parameter as shown in figure 4. The behavior of these quantities is known from the Mie scattering theory.

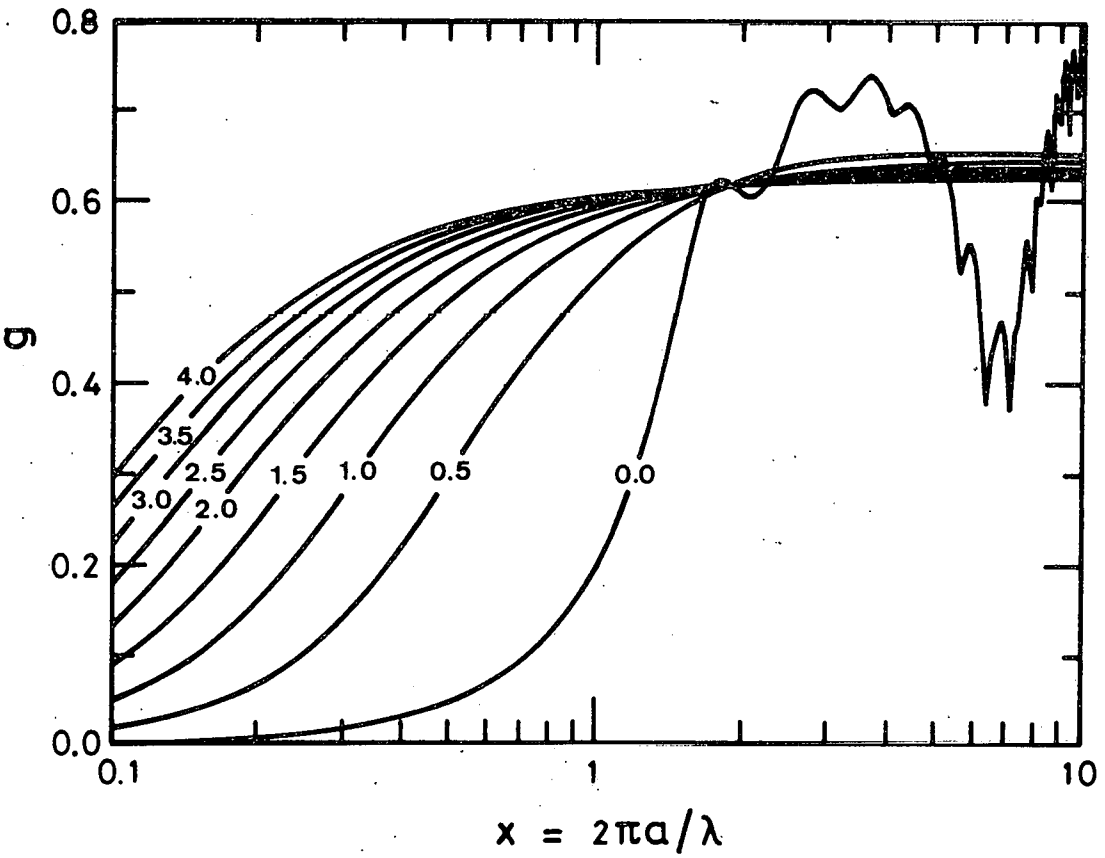

Fig. 3.- Asymmetry factor g as a function of the Mie size parameter for values of b ranging from 0.0 to 4.0 (see equations 3 and 4).

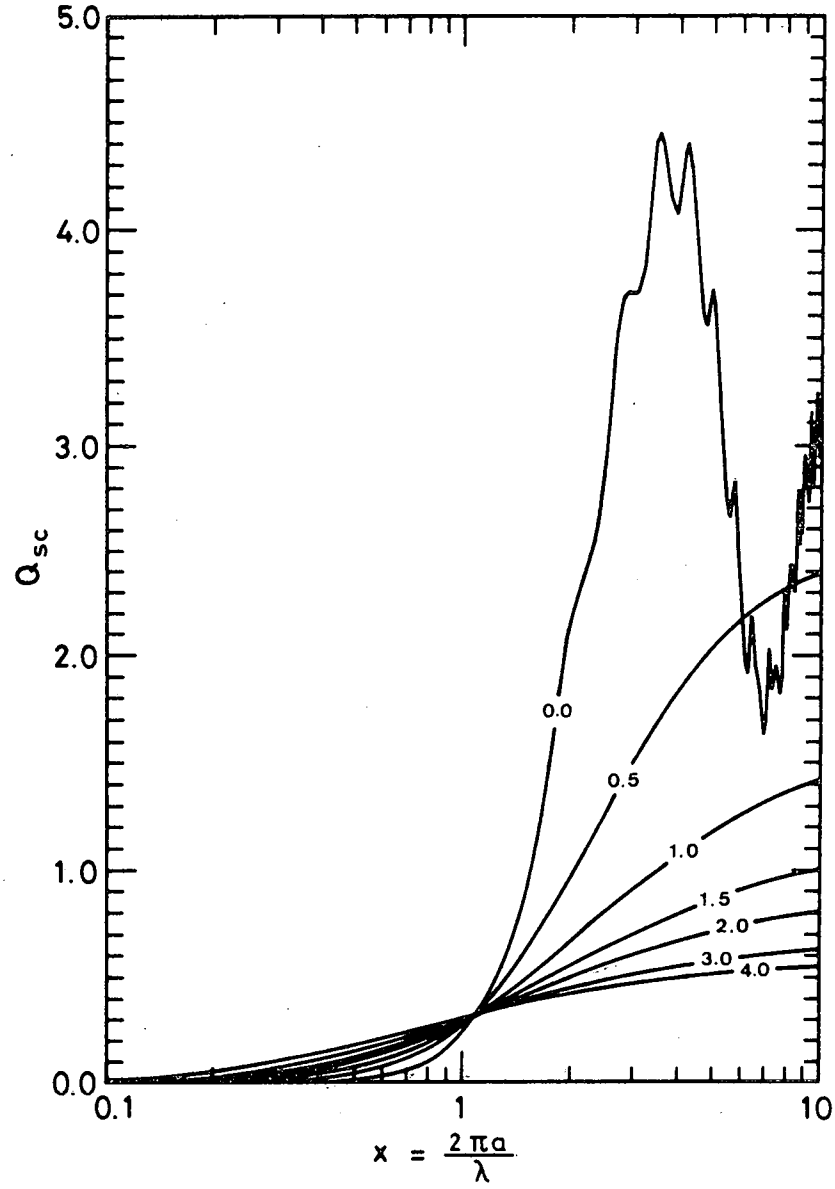

Fig. 4.- Scattering efficiency versus Mie size parameter for b values from 0.0 to 4.0 (see equations 2, 3 and 4).

EXPERIMENTAL DETAILS

The balloon flight from which the data presented here were retrieved took place on October 15, 1980, the tropopause height being at 11.4 km. The gondola floated at 37.6 km altitude and was equipped with seven Hasselblad EL 500 cameras with 80 mm focal length lenses and 70 mm films. Four of them were looking forward, one being loaded with colour EPR 475 Kodak film, and three in the opposite direction. The six black and white cameras had by opposite pair : Wratten filters nr. 47 (440 nm) and 25 (650 nm) with Plus X Kodak film and filters nr. 87 with Kodak aerographic 2424 film (860 nm). In order that the sun images be in the dynamic range of the film, neutral density screens made of exposed and processed sheet films were placed at 60 cm from the lenses with their lower edge placed a few centimeters above the optical axis. Before flight, step wedges, inconel filters and samples of the neutral density screens illuminated in parallel light were recorded by each camera in the laboratory. After the flight, the Plus X films were processed using the Kodak D 76 developper (γ = 1) and the infra-red sensitive film was processed in the Kodak D19 developper (γ = 2.3). The dynamic range of this last film is to small to usefully record simultaneous sun and limb images so that its absolute calibration was derived from the comparison of optical densities due to quasi pure Rayleigh scattering observed 180° from the sun in the three colours above 30 km altitude. The absolute calibration in blue and red light was based directly on solar images. The colour, blue, red and infrared camera settings (aperture, speed) were respectively : f/11, 1/125 sec; f/8, 1/250 sec; f/8, 1/250 sec; f/8, 1/125 sec. As soon as the gondola could be sun oriented, pictures were taken during ascent and later during the float period. Its sun sensor remaining locked on the sun, the gondola was then rotated about its vertical axis so that the cameras could record earth limb images 65, 115, 180, 245 and 295 degrees from the solar azimuth. The whole horizon scan was performed in a short

time, from 1608 to 1618 hrs GMT, during which atmospheric illumination conditions changed very little. The latitude and longitude were respectively 1°E and 44°N. The average solar azimuth and elevation angles were respectively equal to 248° and 9.3°. The optical densities were measured on three tracks per frame normally to the horizon by means of a Jarrell-Ash micro-densitometer and subsequently converted into radiance, in units of solar radiance, versus altitude of the grazing line of sight every 200 meters. Each photograph allows an horizontal angular coverage equal to about 34°.

RESULTS

The observed limb radiance values are presented versus the altitude of closest approach of the line of sight to the earth surface (sea level) for 440 nm, 650 nm and 860 nm and for various scattering angles in the parts a of figures 5, 6 and 7 respectively.

The comparison of the vertical radiance profiles observed at small scattering angles in red light eleven days before, less than one months[10] and five months after Mount St. Helen's eruption shows several characteristic points. A radiance enhancement peaking at 17 km altitude still exists on October 15, 1980, by a factor of almost three relative to the preeruption value. Above 22 km altitude the radiance has returned to values close to what it was on May 7, 1980. This suggests that the heavy layer observed over England on June 6 and 7[11] and on June 5[10] over France constituted the main body of the material injected in the stratosphere by the volcano. Over 5 months, that layer would then have spread in altitude and its center of gravity would have moved upwards by approximately two kilometers, this being perhaps related wich air heating through sunlight absorption by the aerosols.

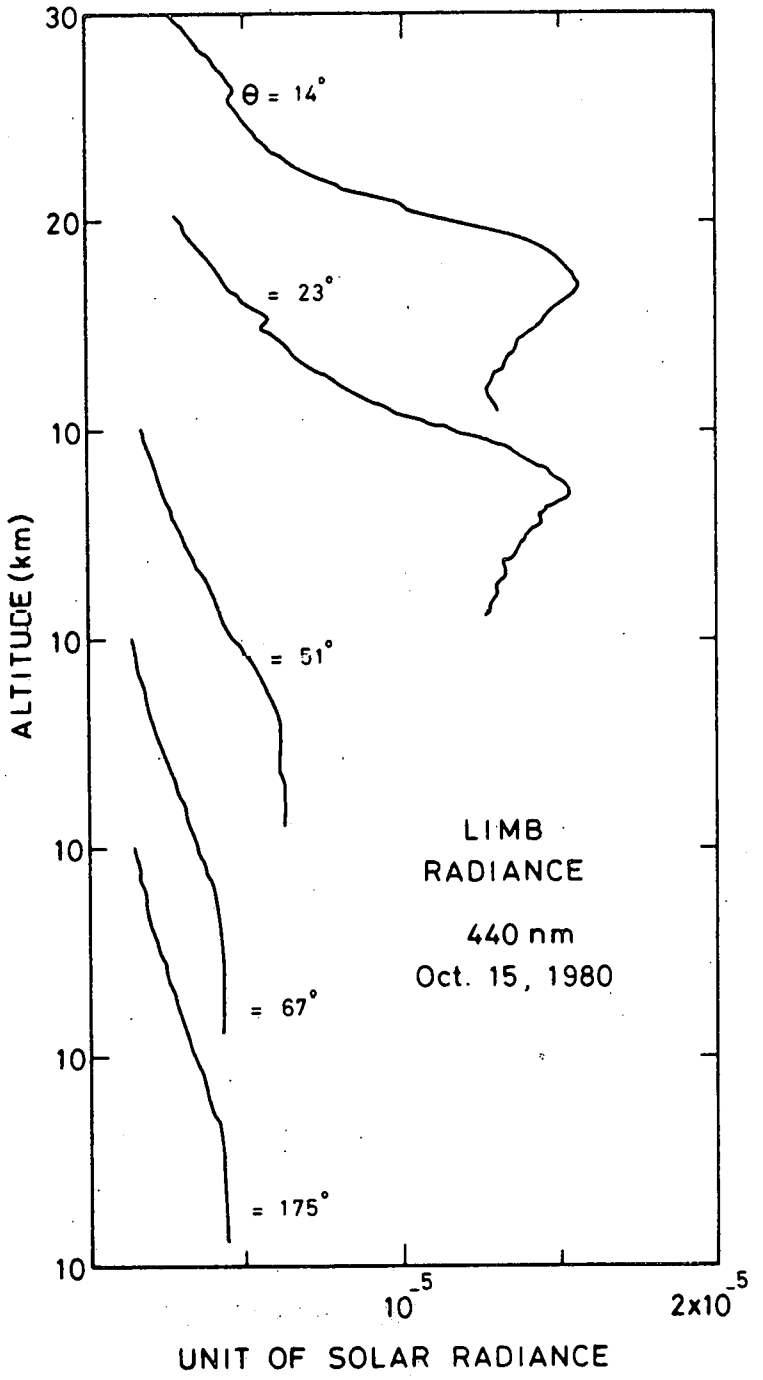

Fig. 5a.- Integrated radiances, R, along the line of sight at 440 nm versus grazing altitude and for various scattering angles, θ. Each successive lower curve is desplaced by 10 km altitude from the one above. Radiance is expressed unit in of solar radiance.

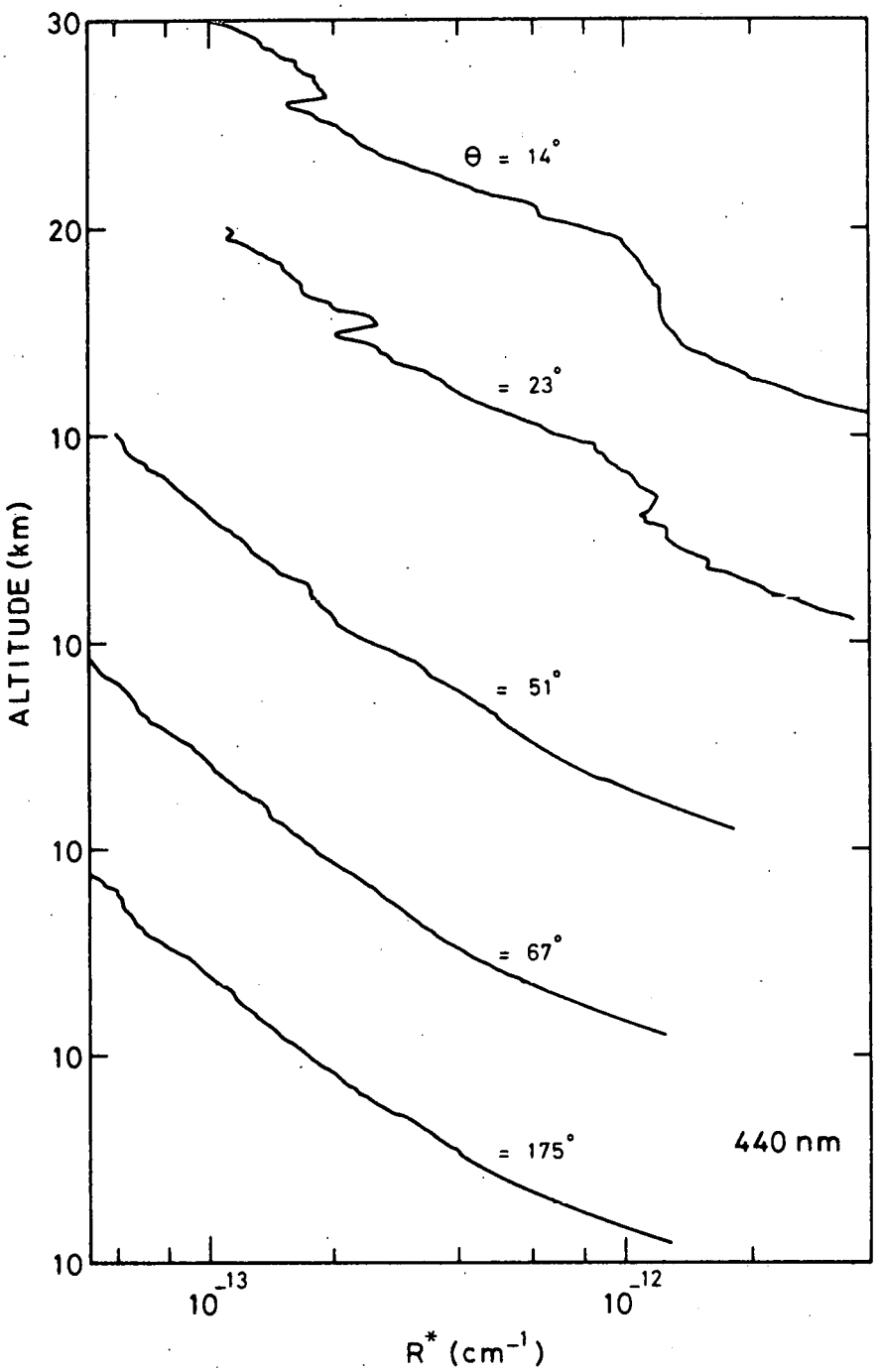

Fig. 5b.- Inverted in situ radiances, R*, versus altitude at 440 nm. Each successive lower curve is desplaced by 10 km altitude from the one above. Radiance is expressed in unit of solar radiance.

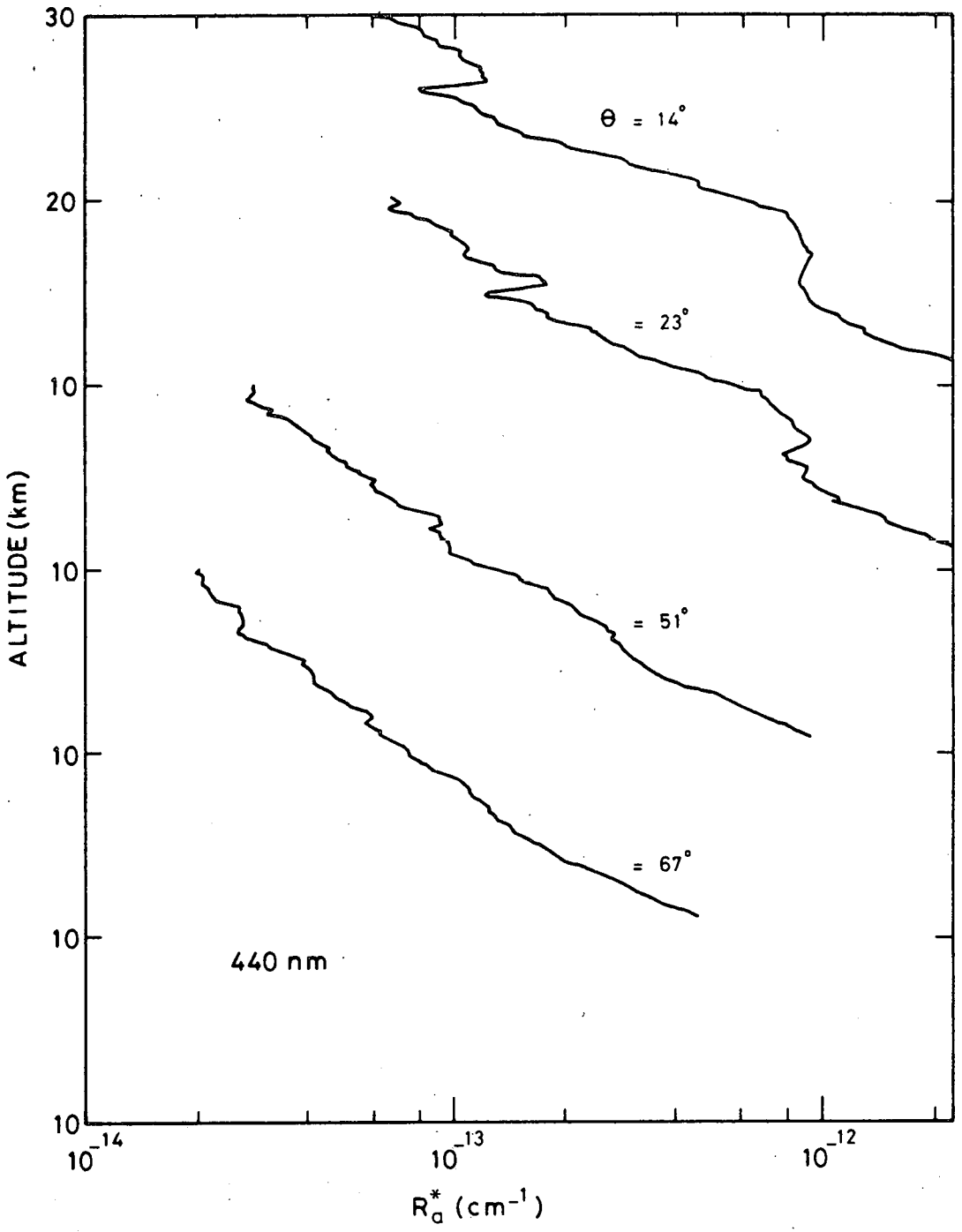

Fig. 5c.- In situ radiances due to aerosols, R^*_a, versus altitude at 440 nm. Each successive lower curve is desplaced by 10 km altitude from the one above. Radiance is expressed in units of solar radiance.

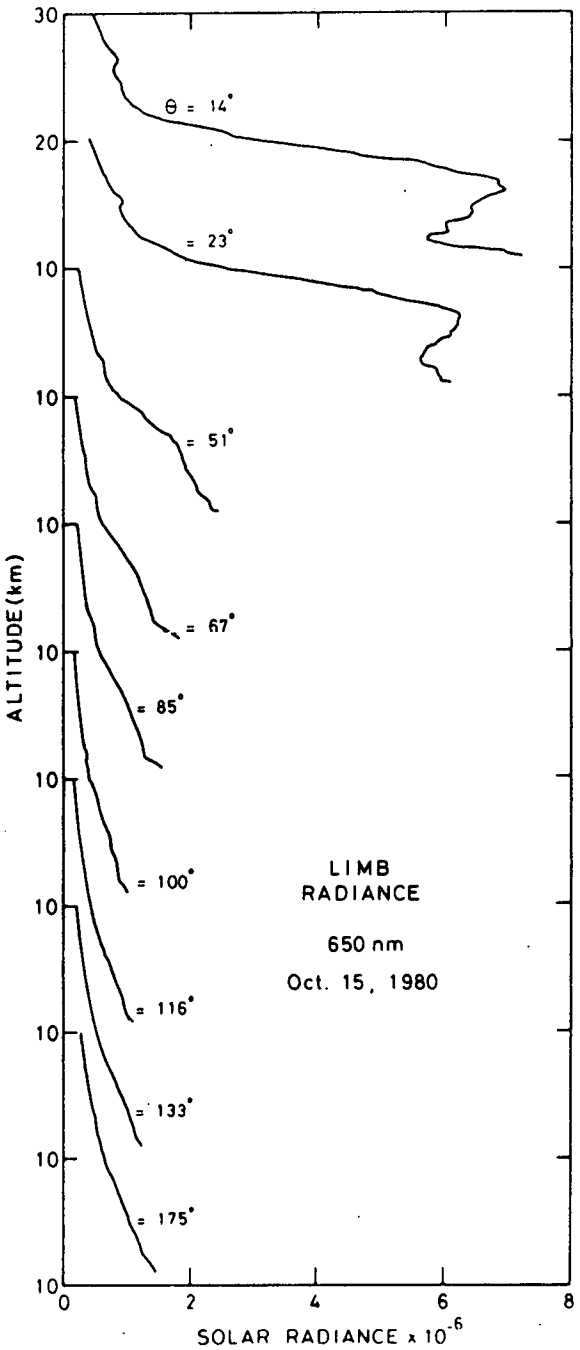

Fig. 6a.- Integrated radiance, R, along the line of sight at 650 nm versus grazing altitude and for various scattering angles, θ. Each successive lower curve is desplaced by 10 km altitude from the one above. Radiance is expressed unit of solar radiance.

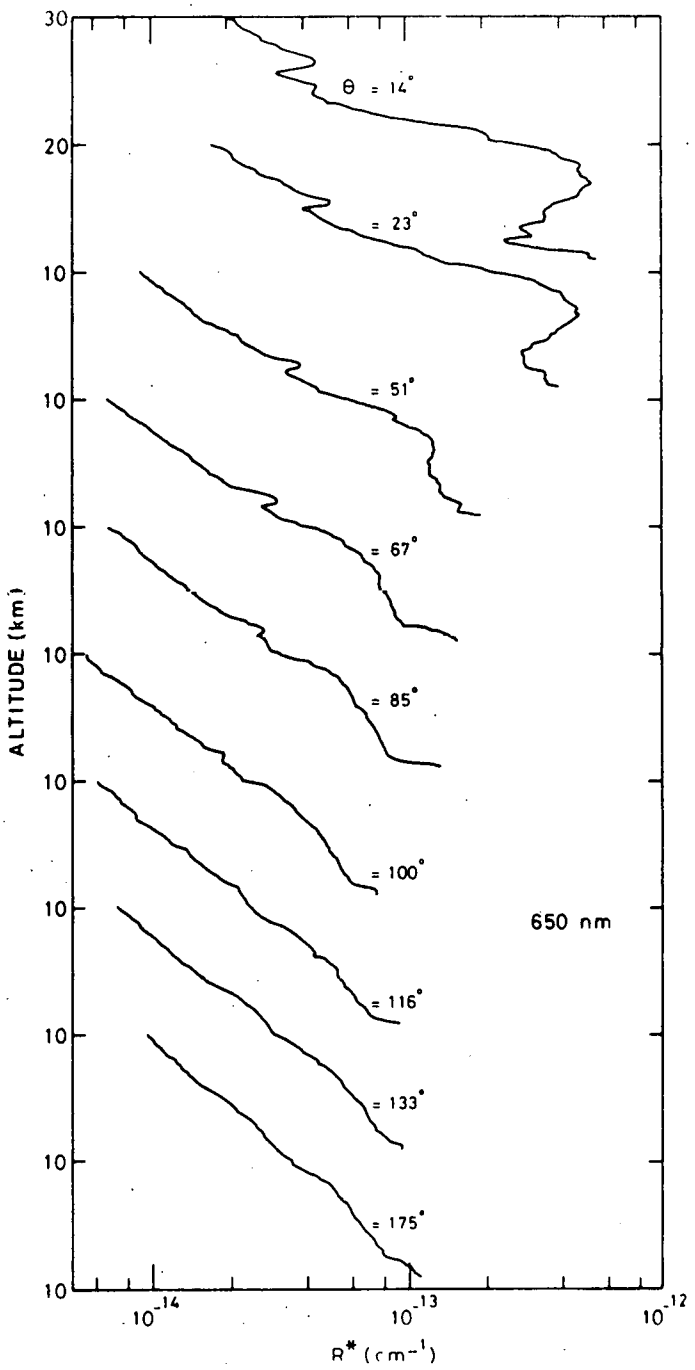

Fig. 6b.- Inverted in situ radiances, R*, versus altitude at 650 nm. Each successive lower curve is desplaced by 10 km altitude from the one above. Radiance is expressed in unit of solar radiance.

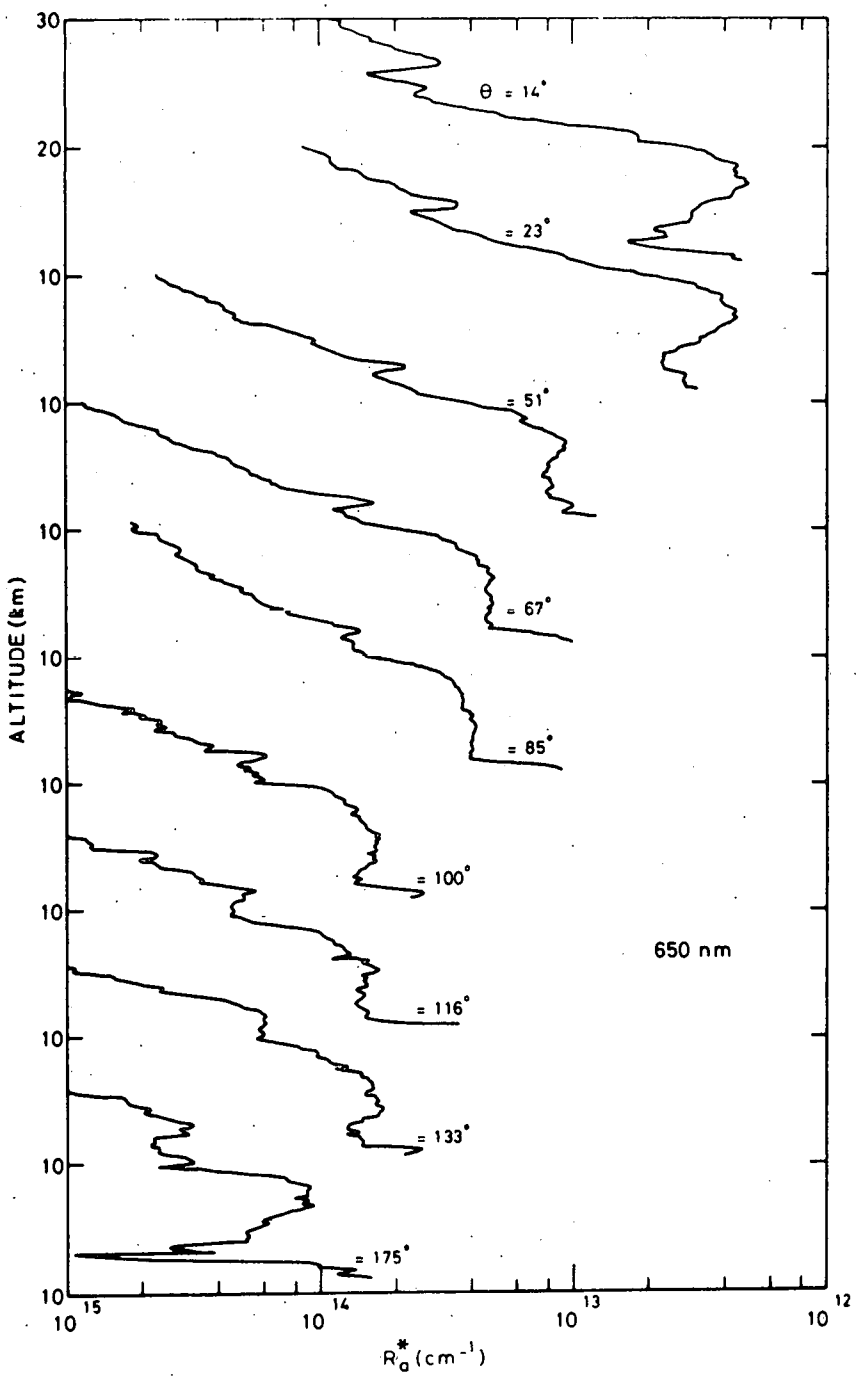

Fig. 6c.- In situ radiances due to aerosols, R^{*}_{a}, versus altitude at 650 nm. Each successive lower curve is desplaced by 10 km altitude from the one above. Radiance is expressed in units of solar radiance.

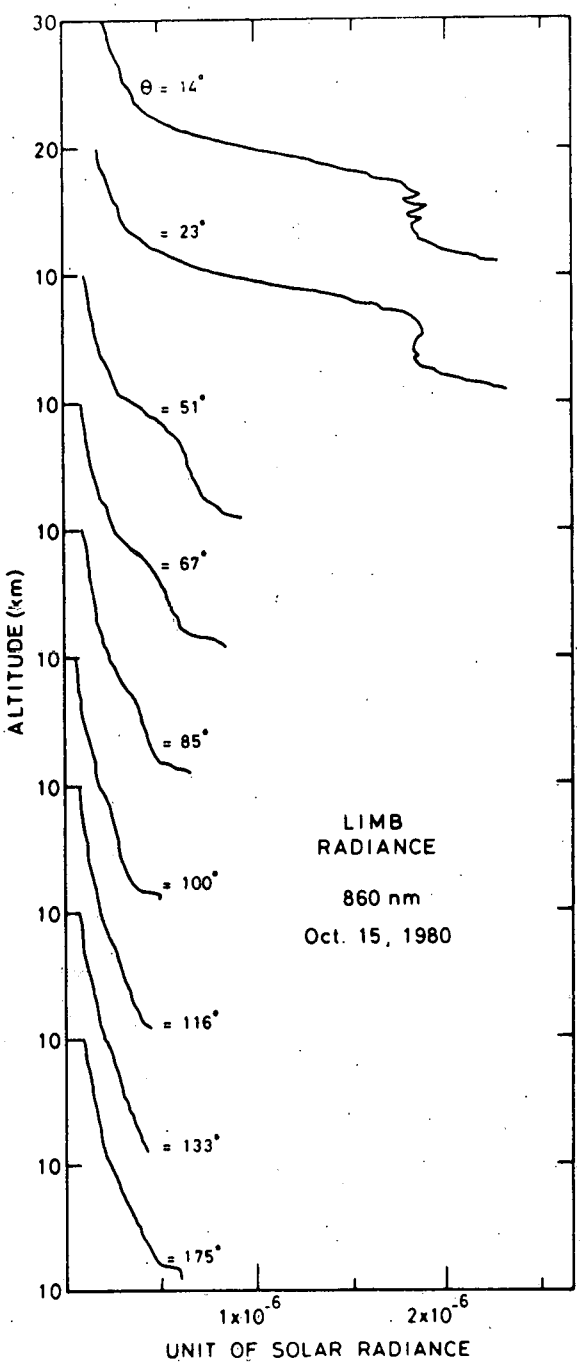

Fig. 7a.- Integrated radiances, R, along the line of sight at 860 nm versus grazing altitude and for various scattering angles, θ. Each successive lower curve is desplaced by 10 km altitude from the one above. Radiance is expressed unit of solar radiance.

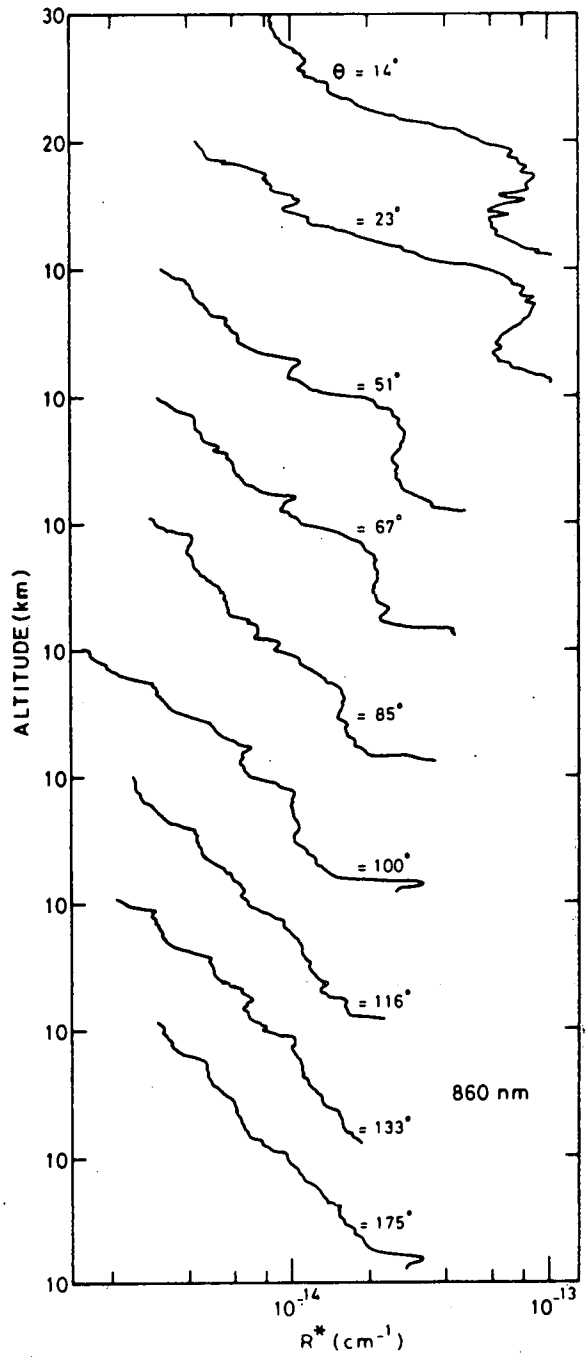

Fig. 7b.- Inverted in situ radiances, R*, versus altitude at 860 nm. Each successive lower curve is desplaced by 10 km altitude from the one above. Radiance is expressed in unit of solar radiance.

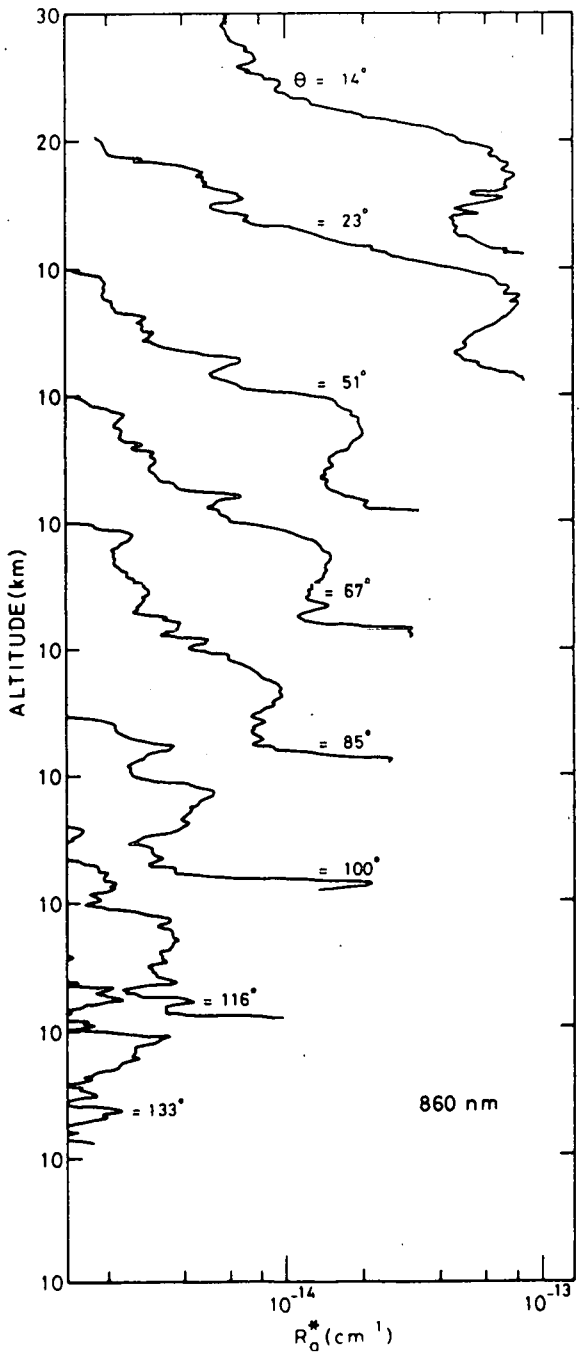

Fig. 7c.- In situ radiances due to aerosols, R_a^*, versus altitude at 860 nm. Each successive lower curve is desplaced by 10 km altitude from the one above. Radiance is expressed in units of solar radiance.

The inspection of the various photographs taken around the vertical axis of the gondola reveals the presence of the 17 km layer at all azimuth angles. Above 20 km altitude a well defined one kilometer thick layer is readily seen on the pictures. Such thin well separated features have been observed on each of our previous flights and have most probably no relation with volcanic activity. They belong to the "natural" stratospheric aerosol. In this particular case the layer is present towards the South from the gondola and absent towards the North. Its altitude is at 22 km from 125° azimuth counted clockwise from the geographic North to about 220° where it begins to rise up to about 25 km at 250° where it splits and becomes non visible. Particulate matter is also present above what we call here the 22 km layer. With respect to the horizontal homogeneity, the study of the aerosol direct sunlight scattering versus scattering angles can be performed safely for the 17 km layer; for higher altitudes some prudence must be exercised.

In order to usefully perform the angular study, the along the lines of sight integrated radiances are inverted. Standard[22] ozone and air distributions and their respective absorption cross sections[23,18] were used for this purpose. The in situ radiance values, R^*; in unit of solar radiance and per cm along the line of sight at the tangent altitude are presented in the parts b of figures 5, 6 and 7. The R^* values at 650 nm (fig. 6b) show at $\theta = 175°$ an exponential dependence versus altitude, as expected, on which some structure and noise is superimposed. At 860 nm (figure 7b) in the backward hemisphere where aerosols are expected to bring a small contribution and particularly at 30 km altitude, the variation of R^* with θ fits well the Rayleigh phase function giving confidence in the very low contribution from the earth albedo to the observed signal. This is not surprising since the average cloud deck radiance measured at depression angles from 5 to 15° ranges from 7×10^{-7} to 6×10^{-7} of the solar radiance at respective azimuths from 0° to 180° from the sun. At $\theta = 14°$ and 17 km altitude the aerosol contribution is about fourteen times the Rayleigh contribution.

At 650 nm (fig. 6b) also the Rayleigh phase function can be fitted to the radiance variation observed in the backward hemisphere at 30 km altitude. In this case however the average cloud radiance varies from 6×10^{-6} near the sun azimuth to 6×10^{-7} elsewhere. In the forward direction the aerosol contribution to the radiance is 10.8 times the Rayleigh contribution at 17 km. At 440 nm, Rayleigh scattering dominates even if at $\theta = 14°$ it still appears to be five times smaller than aerosol scattering at 17 km. At $\theta = 175°$, R^* grows faster than exponentially at altitudes below 20 km. Multiple scattering plays here an important role since the Rayleigh optical thickness on the tangent line of sight reaches unity at 20 km already. This occurs at 9 km and at ground level for 650 and 860 nm respectively. In addition the average cloud deck radiance is very high in blue light varying from 1.6×10^{-5} near the sun direction to 10^{-6} of the solar radiance elsewhere. The data obtained in blue light can then only be used with caution and at small scattering angle. The situation here is different from that in balloon borne aureole observation[24] due to the low solar elevation used here.

The parts c of figures 5, 6 and 7 present the in situ radiance due to aerosols R_a^* which has been obtained by subtracting Rayleigh scattering R_M^* due to air. R_M^* is evaluated from R^* at $\theta = 175°$ following the "clean air" procedure currently used in lidar work[25]. R_M^* is then adapted for the various scattering angles considered according to the molecular phase function[18].

INTERPRETATION

The angular dependance of R_a^* has been fitted to the variation of the scattered light intensity versus θ computed for various values of the asymmetry factor g of the Henyey-Greenstein function. The plots are shown in figures 8a, b and c for the three wavelengths. In blue light a few values of θ give usefull results. For the reasons discussed

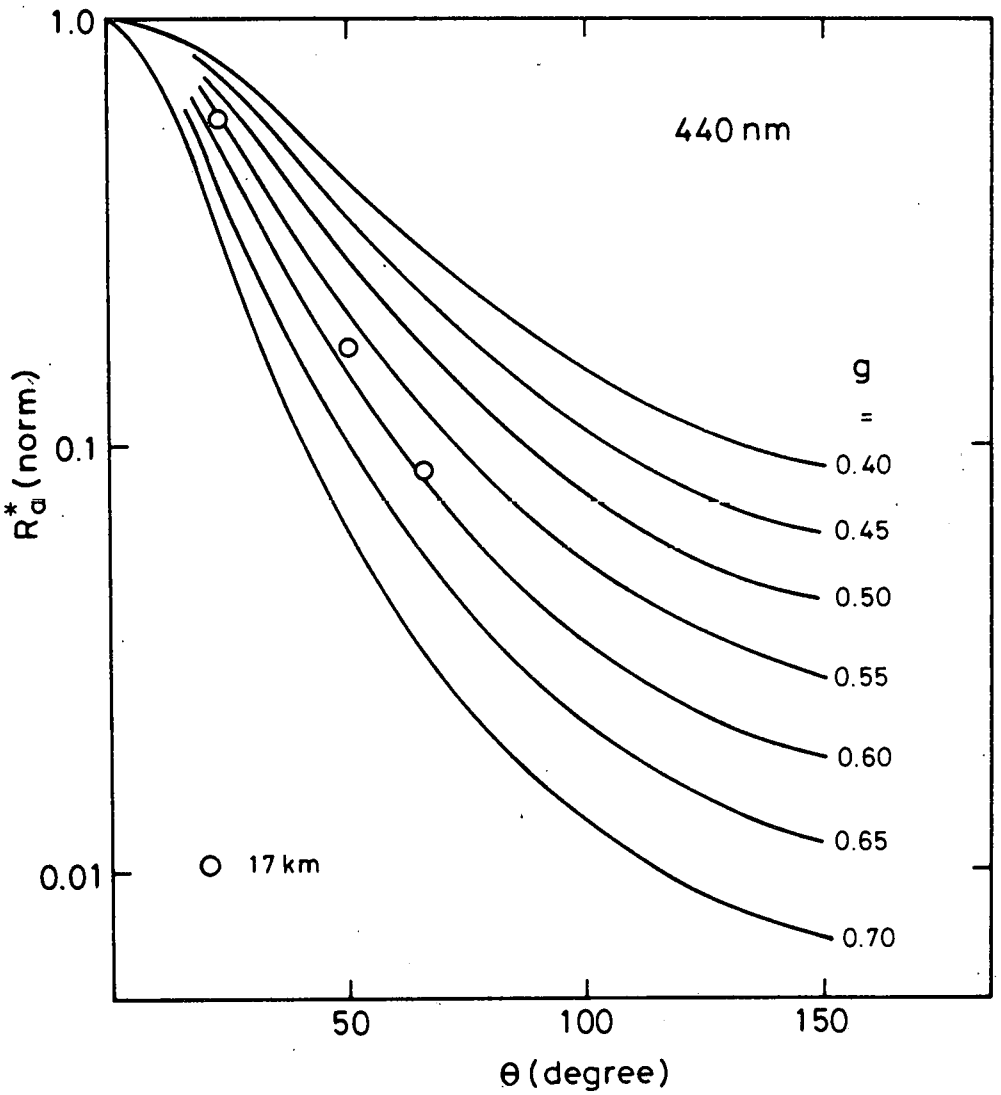

Fig. 8a.- Henyey-Greenstein phase functions of the radiance versus scattering angles, normalized at $\theta = 0°$ and for various values of the asymmetry factor, g. The experimental data points are shown at the three altitudes studied and for the three wavelengths : a, 440 nm; b, 650 nm; c, 860 nm.

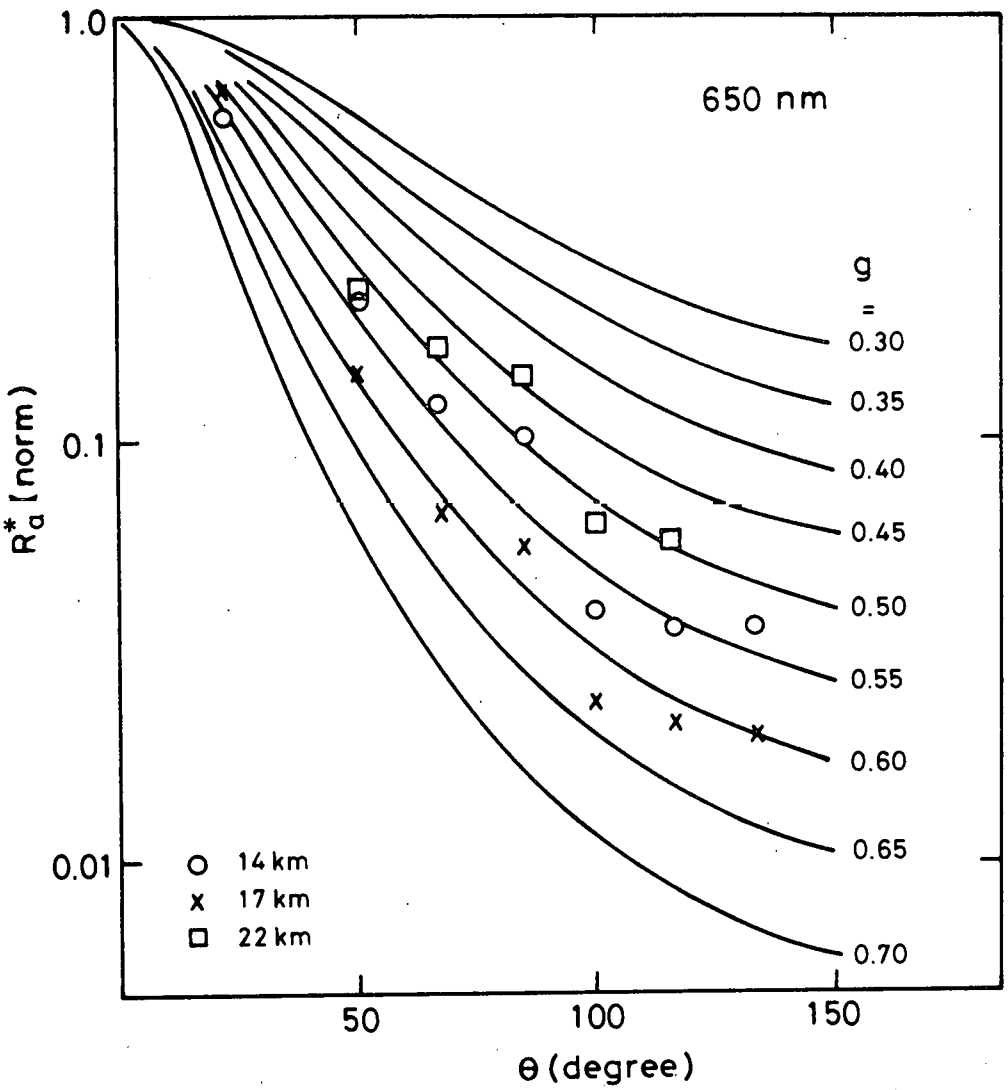

Fig. 8b.- Henyey-Greenstein phase functions of the radiance versus scattering angles, normalized at $\theta = 0°$ and for various values of the asymmetry factor, g. The experimental data points are shown at the three altitudes studied and for the three wavelengths : a, 440 nm, b, 650 nm; c, 860 nm.

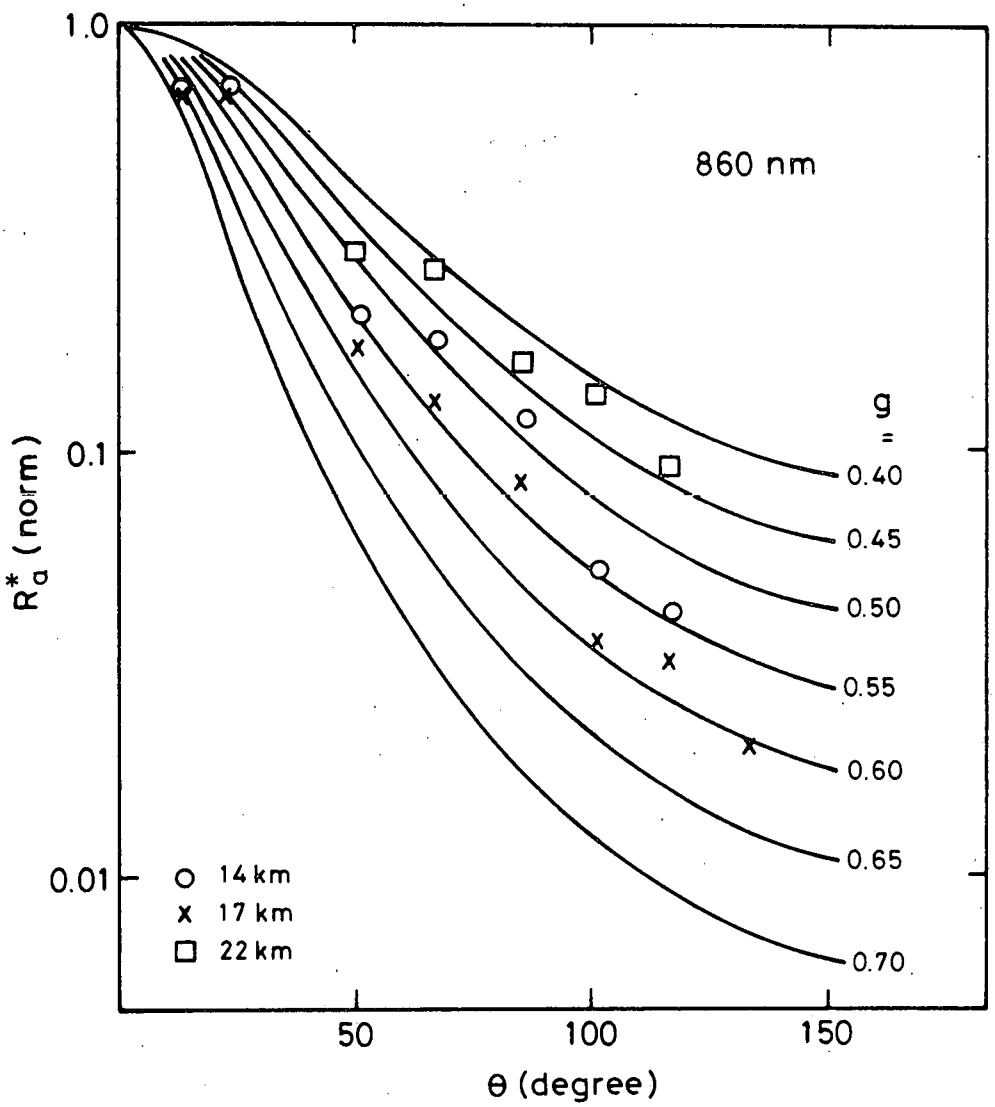

Fig. 8c.- Henyey-Greenstein phase functions of the radiance versus scattering angles, normalized at $\theta = 0°$ and for various angles of the asymmetry factor, g. The experimental data points are shown at the three altitudes studied and for the three wavelengths : a, 440 nm; b, 650 nm; c, 860 nm.

earlier values for the 22 km layer have only been considered for θ from 51° to 116°.

The asymmetry factors determined in this fashion are listed in table 1 as well as the optical scattering extinction coefficients Q_s n σ. The values at 440 nm are only indicative but have not been used since a model taking into account the measured cloud radiances indicates a non negligeable contribution of the albedo to the limb radiance. From the model, this is negligeable at the larger wavelengths. The observed g values, taking into account that it is most probably slightly higher than 0.6 at 440 nm, tend to indicate that a value of the real index of refraction equal to 1.55, as currently used in models[26], is observed here. This value will then be used to deduce the size parameters x. Their variation with λ from 650 to 860 nm leads to the table 1 listed a and b values characterizing the size distribution. Eventually, the scattering efficiency Q_s can be deduced from a and b following the Mie scattering theory[20].

With the data available, there is of course another method of determining ΣQ_s nσ. From the air σ values[18] and from the air number density n_{air} taken from a model[22] (mid-latitude, spring-fall) $(n\sigma)_{air}$ can be evaluated. The R^*_M values determined at θ = 175° by the "clean air" method[25] are compared with the R^*_a measured and by taking into account the air and aerosols phase functions the values of $(\Sigma Q_s\ n\sigma)_{AM}$ for the aerosols are deduced. They are also listed in Table 1.

The absolute particle distribution shown in figure 9 for the three altitudes considered is based only on the geometrical extinction coefficient $\Sigma n\sigma$ at 860 nm for two reasons. In infrared light, the albedo contribution to the measurement is negligeable while it is maximum in blue light and in the inversion of R leading to R^* the correction for the absorption by O_3, of which a standard vertical distribution had to be used, is the largest in red light. This is supported by the discrepancy

TABLE 1.- Summary of results. The following quantities are given for three characteristic altitudes : g, the asymmetry factor of the phase function; $\Sigma Q_s n\sigma$, the optical aerosol scattering extinction deduced from observed radiances; $(\Sigma Q_s n\sigma)_{AM}$, the optical aerosol scattering extinction deduced from comparison with the molecular scattering extinction; Q_s, the scattering efficiency factor; $\Sigma n\sigma$ and $(\Sigma n\sigma)_{AM}$, the geometric scattering extinctions; a, b, the size distributions parameters; V, the total volume of particles per cubic centimeter of air at the respective altitudes.

	14 km	17 km	22 km
g_{440}	-	0.6	-
g_{650}	0.55	0.60	0.50
g_{860}	0.52	0.56	0.45
$\Sigma Q_s n\sigma_{440}$ (cm^{-1})	-	3.2×10^{-8}	-
$(\Sigma Q_s n\sigma_{440})_{AM}$ (cm^{-1})	-	1.5×10^{-8}	-
$\Sigma Q_s n\sigma_{650}$ (cm^{-1})	9.4×10^{-9}	1.0×10^{-8}	2.9×10^{-9}
$(\Sigma Q_s n\sigma_{650})_{AM}$ (cm^{-1})	6.0×10^{-9}	5.8×10^{-9}	1.5×10^{-9}
$\Sigma Q_s n\sigma_{860}$ (cm^{-1})	1.9×10^{-9}	2.7×10^{-9}	9.3×10^{-10}
$(\Sigma Q_s n\sigma_{860})_{AM}$ (cm^{-1})	2.4×10^{-9}	3.1×10^{-9}	9.2×10^{-10}
$Q_{s\ 440}$	-	0.8	-
$Q_{s.\ 650}$	0.14	0.52	0.1
$Q_{s\ 860}$	0.10	0.35	0.05
$\Sigma n\sigma_{440}$ (cm^{-1})	-	4×10^{-8}	-
$(\Sigma n\sigma_{440})_{AM}$ (cm^{-1})	-	1.9×10^{-8}	-
$\Sigma n\sigma_{650}$ (cm^{-1})	6.7×10^{-8}	1.9×10^{-8}	2.9×10^{-8}
$(\Sigma n\sigma_{650})_{AM}$ (cm^{-1})	4.3×10^{-8}	1.1×10^{-8}	1.5×10^{-8}
$\Sigma n\sigma_{860}$ (cm^{-1})	1.9×10^{-8}	7.7×10^{-9}	8.9×10^{-9}
$(\Sigma n\sigma_{860})_{AM}$ (cm^{-1})	2.4×10^{-8}	8.9×10^{-9}	8.8×10^{-9}
a (μm)	0.042	0.15	0.045
b	3.6	0.6	1.8
V (cm^3)	1.8×10^{-13}	1.5×10^{-13}	7.0×10^{-14}

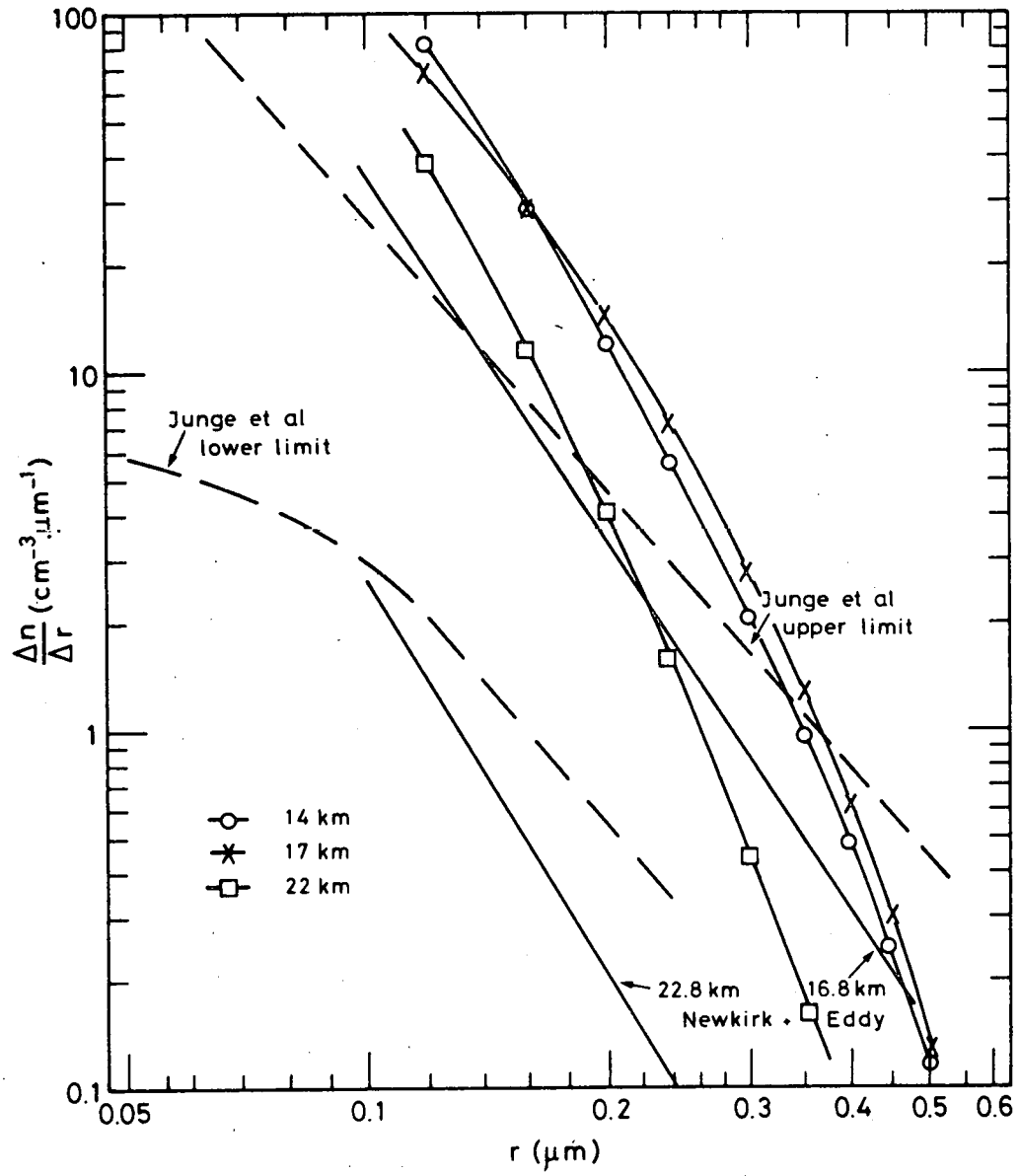

Fig. 9.- Number of particles per cm^{-3} versus their radii and per micron size interval for three characteristic altitudes : 14, 17 and 22 km. Two previous data sets[8, 24] are shown for the sake of comparison.

observed at shorter wavelength between the extinctions determined from the observed radiances and those determined by comparison with the molecular scattering. The agreement is very good at 860 nm. The Mie scattering theory has, in addition, the best chances to be valid, even if the particles do not exhibit a perfectly spherical and smooth shape, at small values of the size parameter.

DISCUSSION

In order to characterize the particle size range to which the measurements presented here are sensitive, the cumulative asymmetry factor, g, has been computed by adding successively the particles radii slices starting with the smallest particles. The results are shown in figures 10 and 11 for 0.65 μm and for 0.86 μm respectively. This shows that for particles smaller than 0.04 μm and larger than 0.4 μm, g is not significantly affected.

Our particle distributions are compared in figure 9 with the upper and lower limits deduced from in situ sampling[8] and with two extreme values resulting from solar aureole measurements[24]. The results obtained here fall within the range of those data except for particles smaller than 0.2 μm radius where the upper limit given by Junge et al[8] is exceeded. As mentionned earlier the aerosols below 20 km are here still in volcanically perturbed conditions. On the other hand the collection efficiency of in situ sampler might be reduced for small particles. It should also be mentionned that our distributions are steeper especially at large radii. This effect is less pronounced in the comparison with the aureole data. This effect appears to be due to the small values of effective radii obtained here.

An other comparison of our data, shown in fig. 12, can be made with the total number of particles with a radius larger than 0.15 μm

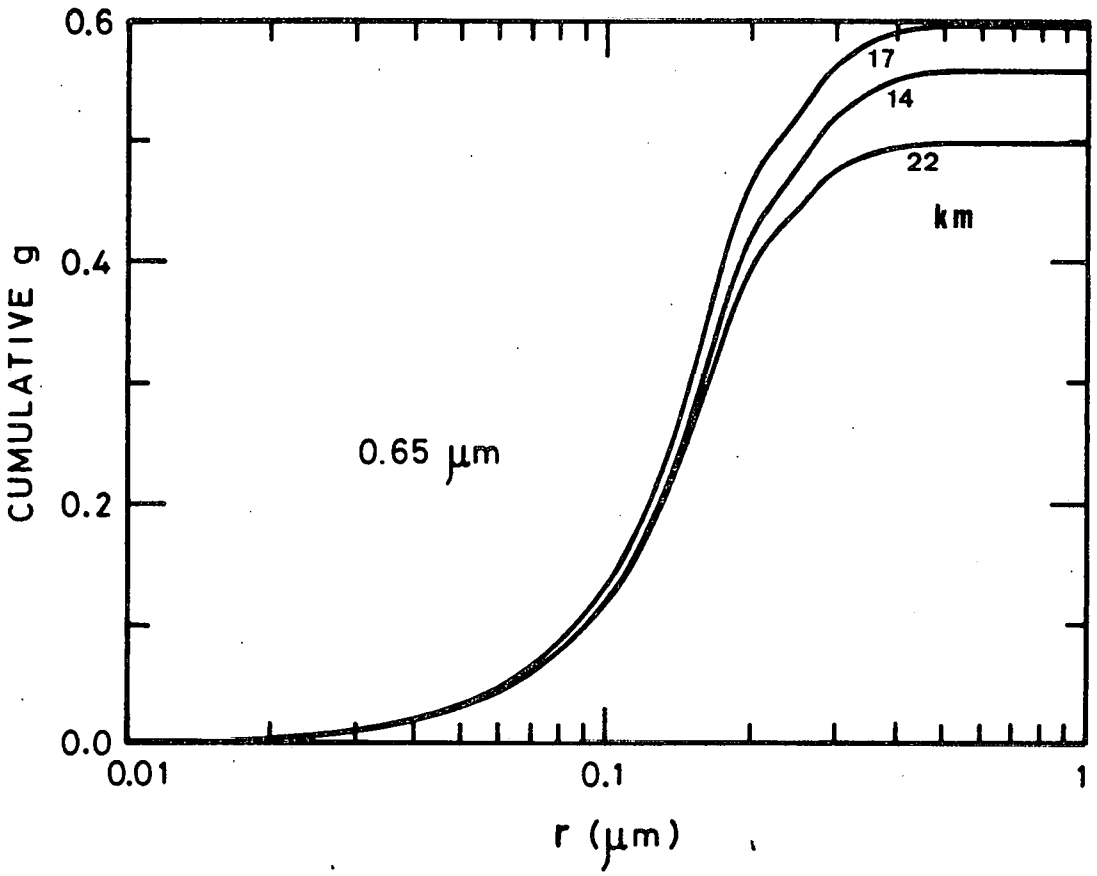

Fig. 10.- Build up of the asymmetry factor g of the phase function when, from the smallest particle sizes, successive slices of the distribution are added with increasing particle radii, r. At 650 μ, significant contributions can be considered from 0.03 μm to 0.4 μm radii.

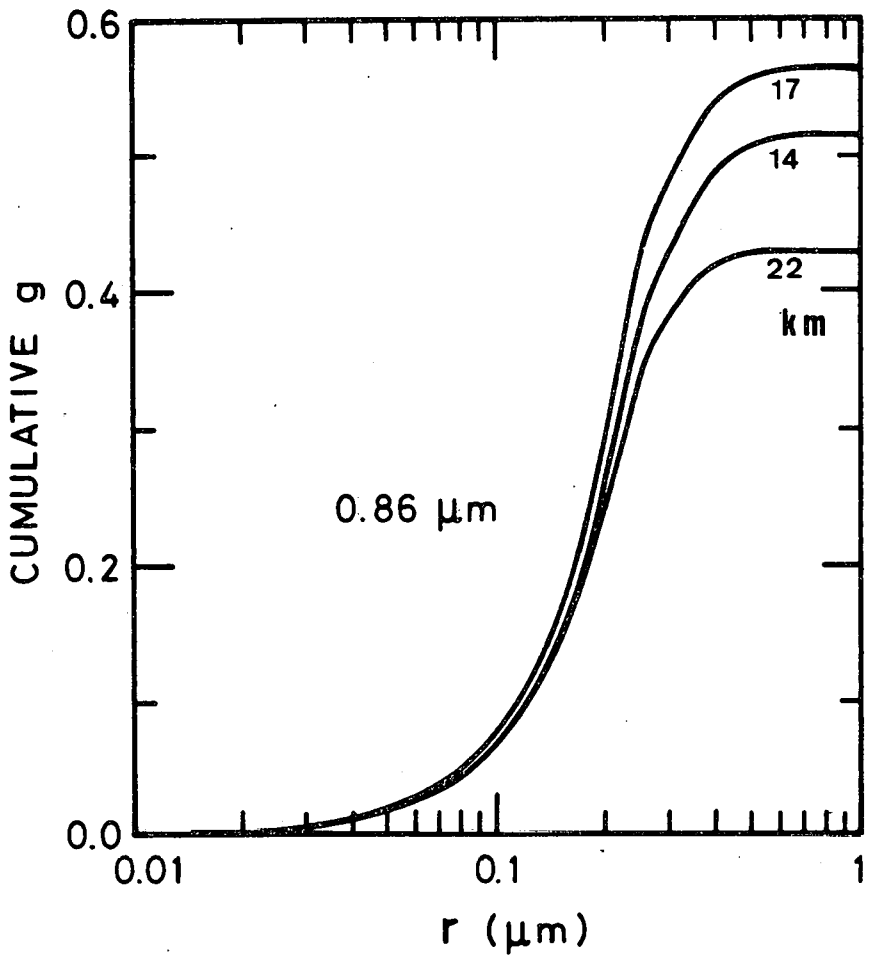

Fig. 11.- Build up of the asymmetry factor g of the phase function when, from the smallest particle sizes, successive slices of the distribution are added with increasing particle radii, r. At 860 nm, significant contribution can be considered from 0.04 to 0.4 μm radii.

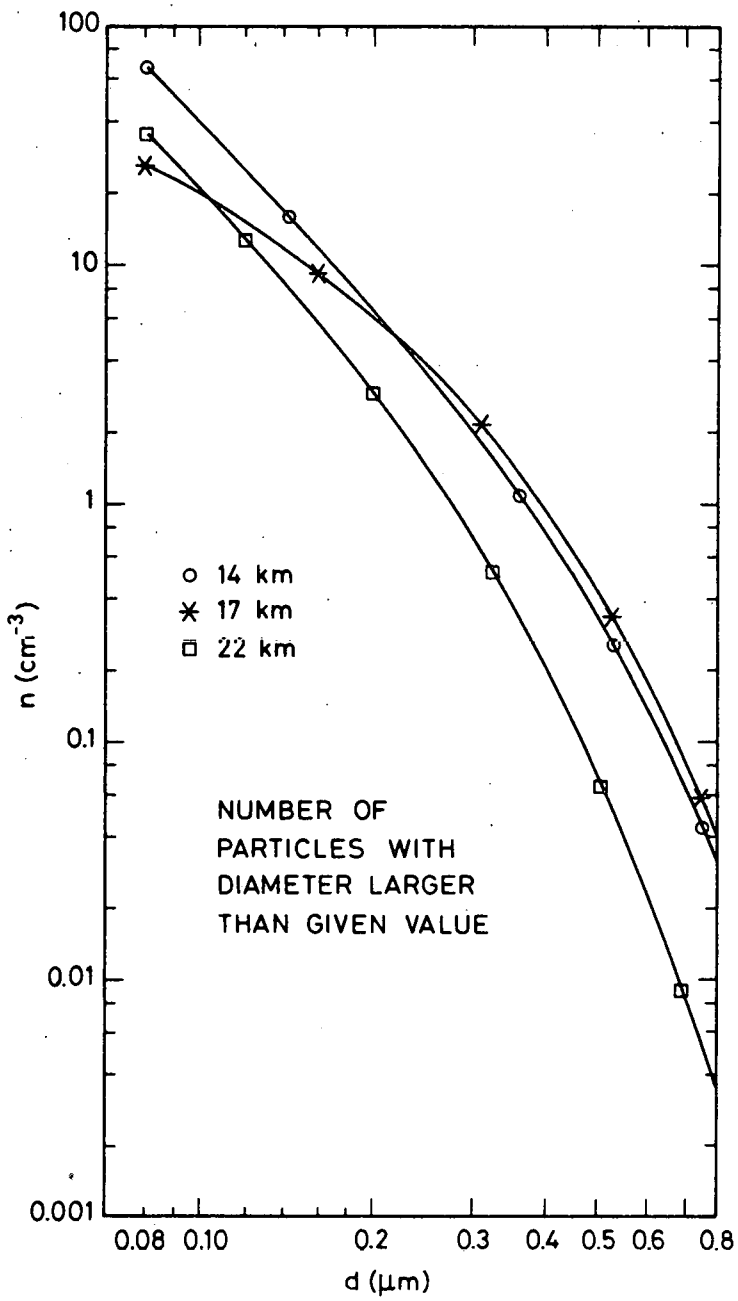

Fig. 12.- Total numbers of particles with diameters larger than given values. The ratio of the number of particles with diameters larger than 0.3 μm to the number of particles with diameters larger than 0.5 μm is larger for the layer at 22 km altitude than for 17 and 14 km altitude indicating the volcanic influence in these two latter cases[32].

obtained by means of balloon borne optical particle counters[27]. The number densities of these particles are found to be from 0.4 to 1.3 particle cm^{-3} in the 14 to 17 km altitude region and from .1 to .9 particle cm^{-3} at 22 km. As already mentionned, the data presented here for 22 km correspond to a low aerosol content above 20 km and lead to 0.7 particle cm^{-3} above 0.15 μm. At 14 and 17 km altitude the values presented in fig. 5 respectively imply 1.9 and 2.1 particle cm^{-3} of particles with radii larger than 0.15 μm. An intercomparison of the two methods would be required to define a possible discrepancy since the aerosols are volcanically enhancened in the present case.

The optical extinction coefficient $Q_s n\sigma$ measured at 1 μm wavelength by the SAM II satellite borne instrument at low aerosol load in July 1979[28] exhibit an almost constant value from 14 to 20 km altitude equal to 10^{-9} cm^{-1}. This compares very favorably with our 860 nm value at 22 km. At 17 and 14 km altitude, the extinction in the present case is 3 and 2 times larger. This can be expected from the volcanic influence which may also explain the larger effective particle radius a at 17 km altitude.

A value of the asymmetry factor g equal to 0.49 ± 0.7 has been measured recently at 633 nm, a wavelength close to 650 nm used here, from 10.7 to 12.8 km altitude in the stratosphere[19]. This value corresponds to our measurement at 22 km where the aerosol is considered to be purely "natural". Since g is larger in the present case at 14 and particularly at 17 km, one of the volcanic influences must then be to increase the g value and if the Mie theory is applicable to increase the particle size as we observe it at 17 km altitude.

From an optical point of view the particle size distribution, of which the shape is of greater interest than the particle concentration for radiative transfer calculations[26], is variable in the stratosphere.

The asymmetry factor, g, is smaller than the constant value (0.7) currently used in models for visible light. Such a high value corresponds to the log normal and Zero Order Logarithmic Distribution. Both have been respectively proposed by Pinnick et al[29] and by Toon and Pollack[26] and are shown on figure 13. They are compared with the model values computed for 16,20 and 30 km altitude by Toon et al[30].

For photochemical models of stratospheric aerosols[31] the variable size distribution will have a role to play. The molecular content of the condensed phase supposed to be oxydized sulfur, water vapor and perhaps other species is not negligeable for the gas phase either since conversion into vapor would lead to volume concentrations in the 10^8 to 10^9 molecules cm^{-3} at altitudes from 15 to 20 km. The volume of the condensed phase observed here is shown in table 1.

The deduced size distribution of particle surface area and the surface collision rate are compared with model values in figure 14. The knowledge of this latter quantity is required in the evaluation of the stratospheric importance of heterogenous chemical reactions.

CONCLUSION

The measurements presented here confirm recent data and provide new information on critical points which are of fundamental importance in the evaluation of the role that stratospheric aerosols can play. A more sophisticated analysis will be further applied on higher quality experimental data since the potentialities of the method presented here appear to be high.

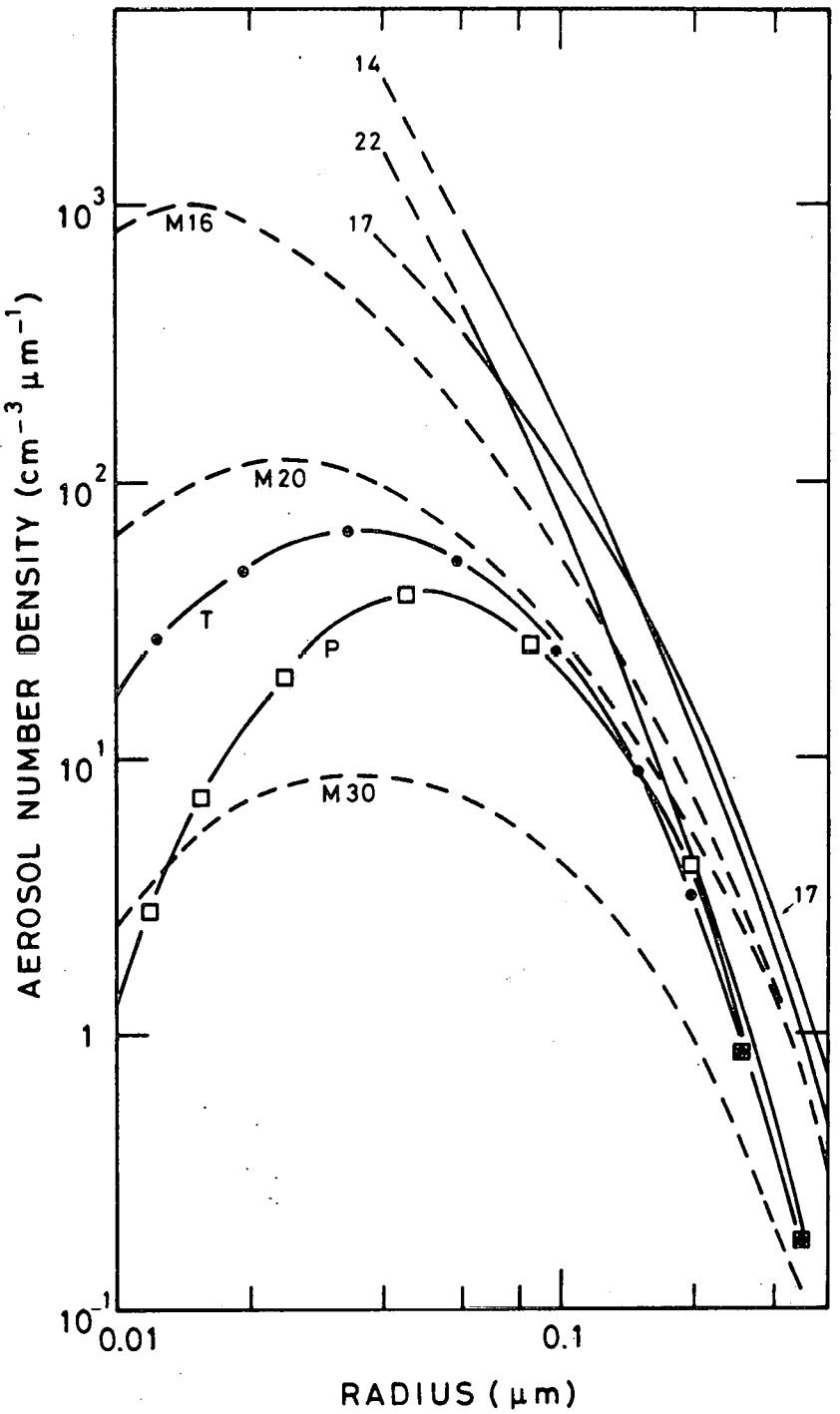

Fig. 13.- Aerosol particle number density per micrometer radius interval versus particle radius for 14, 17 and 22 km. For the sake of comparison, model values[30] are shown for 16, 20 and 30 km altitude (M16, M20, M30). The agreement is reasonably good between the observed values at 17 km and M16. The model size distributions of Pinnick et al[29] and of Toon and Pollack[26] are also shown and are respectively marked P and T in the figure.

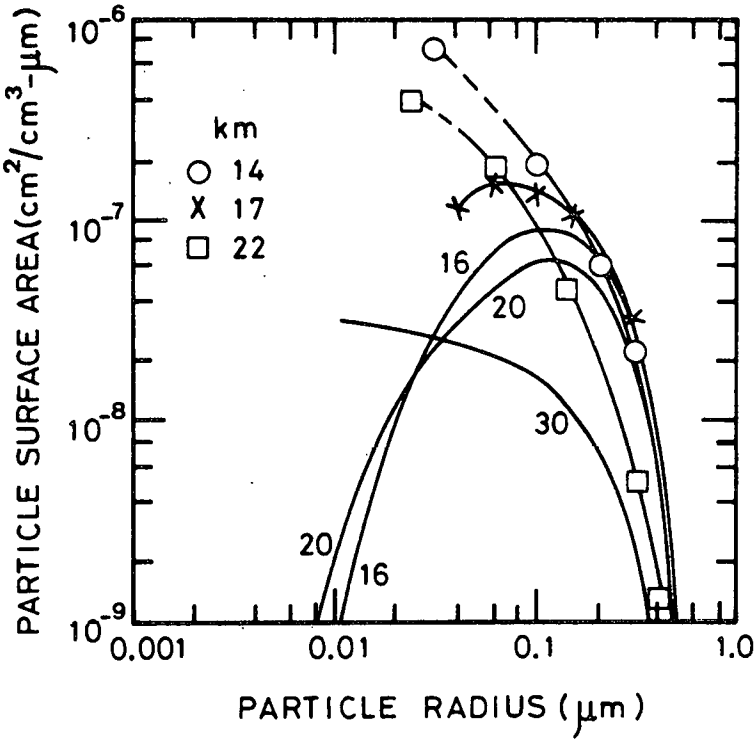
PARTICLE SURFACE AREA(cm²/cm³-μm)
10⁻⁶
10⁻⁷
10⁻⁸
10⁻⁹
km
○ 14
X 17
□ 22
16
20
30
20
16
0.001
0.01
0.1
1.0
PARTICLE RADIUS (μm)

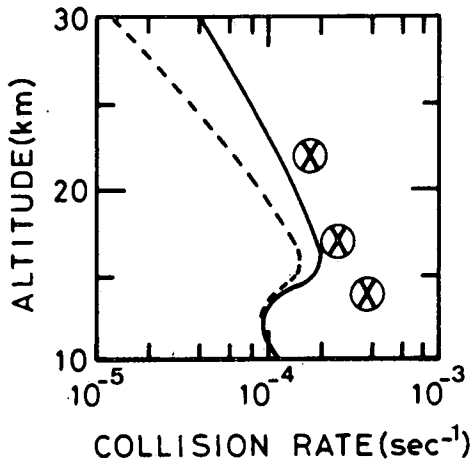
ALTITUDE(km)
30
20
10
10⁻⁵
10⁻⁴
10⁻³
COLLISION RATE(sec⁻¹)

Fig. 14.- The upper part shows the particle surface area distribution versus the particle radius for 14, 17 and 22 km altitude. The model[30] values are shown for 16, 20 and 30 km altitude. In the lower part, the collision rate ($1/4\ s.\bar{u}$), where the average molecular speed $\bar{u}$ is computed for a molecular mass equal to 30 and for typical stratospheric temperatures and where the total particle area is derived from the measurements, is represented by the crossed circles. The dashed and solid lines represent model computed values[33] without and with the effect of meteoritic debris. Further measurements will be required in periods of low volcanic activity to interpret further this comparison. For the time being our measurements support a non negligeable effect of meteoritic debris on the stratospheric aerosols. The high value observed at 14 km relative to the model may possibly show a need for a two dimensional model where the varying tropopause altitude would allow a better comparison with the experiment.

REFERENCES

1. ROZENBERG, G.V., Soviet Physics Uspekhi, 3, 346-371 (1960).
2. DEIRMENDJIAN, D., Rev. of Geophys. and Space Phys., 18, 341-360 (1980).
3. BIGG, E.K., Tellus, 16, 76-83 (1964).
4. VOLZ, F.E. and GOODY, R.M., J. Atm. Sci., 19, 384-406 (1962).
5. GIOVANE, F., SCHUERMAN, D.W. and GREENBERG, J.M., J. Geophys. Res., 81, 5383-5388 (1976).
6. GARRIOTT, O.K., J. Opt. Soc. Amer., 69, 1064-1068 (1979).
7. ROZENBERG, G.V. and NIKOLAEVA-TERESHKOVA, V.V., Izv., Atmospheric and Oceanic Phys., 1, 228-232 (1965).
8. JUNGE, C.E., CHAGNON, C.W. and MANSON, J.E., J. Meteorol., 18, 81-108 (1961).
9. CADLE, R.D. and GRAMS, G.W., Rev. Geophys. Space Phys., 13, 475-501 (1975).
10. ACKERMAN, M., LIPPENS, C. and LECHEVALLIER, M., Nature, 287, 614-615 (1980).
11. THOMAS, L., CHALONER, C.P. and BHATTACHARYYA, S.K., Nature, 289, 473 (1981).
12. REITER, R., JÄGER, H., CARNUTH, W. and FUNK, W., Geophys. Res. Lett., 7, 1099-1101 (1980).
13. D'ALTORIO, A., VISCONTI, G., FIOCCO, G., Geophys. Res. Lett., 8, 63-65 (1981).
14. MEIXNER, F.X., GEORGII, H.W., OCKELMAN, G., JÄGER, H. and REITER, R., Geophys. Res. Lett., 8, 163-166 (1981).
15. DANIELSEN, E.F., Science, 211, 819-821 (1981).
16. POLLACK, J.B., Science, 211, 815-816 (1981).
17. LINK, F. and NEUZIL, L., Tables of Light Trajectories in the terrestrial Atmosphere (Hermann, Paris, 1969).
18. PENNDORF, R., J. Opt. Soc. Am., 47, 176-183 (1957).

19. GRAMS, G.W., Geophys. Res. Lett., 8, 13-14 (1981).
20. HANSEN, J.E. and TRAVIS, L.D., Space Sci. Rev., 16, 527-610 (1974).
21. WISCOMBE, W.J., Applied Optics, 19, 1505-1509 (1980).
22. U.S. Standard Atmosphere, 1976, U.S. Government Printing Office, Washington D.C. 20402 - U.S.A.
23. ACKERMAN, M., in Mesospheric models and related experiments, G. Fiocco, Ed. Reidel Publ. Cy. Dordrecht-Holland (1971).
24. NEWKIRK, Jr., G. and EDDY, J.A., J. Atmos. Sci. 21, 35-60 (1964).
25. GRAMS, G. and FIOCCO, G., J. Geophys. Res., 72, 3523-3542 (1967).
26. TOON, O.B. and POLLACK, J.B., J. Appl. Meteorol., 15, 225-246, 1976.
27. HOFMANN, D.G., ROSEN, J.M., PEPIN, T.J. and PINNICK, R.G., J. Atmos. Sci., 32, 1446-1456 (1975).
28. McCORMICK, M.P. et al., Geophys. Res. Lett., 8, 3-4 (1981).
29. PINNICK, R.G., ROSEN, J.M. and HOFMAN, D.J. J. Atmos. Sci., 33, 304-314 (1976).
30. TOON, O.B., TURCO, R.P., HAMILL, P., VIANG, C.S. and WHITTEN, R.C., J. Atmos. Sci., 36, 718-736 (1979).
31. WHITTEN, R.C., TOON, D.B. and TURCO, R.P., Pageophy, 118, 86-127 (1980).
32. HOFMANN, D.J. and ROSEN, J.M., J. Atmos. Sci., 38, 168-181 (1981).
33. TURCO, R.P., TOON, O.B., HAMILL, P. and WHITTEN, R.C., J. Geophys. Res., 86, 1113-1128 (1981).

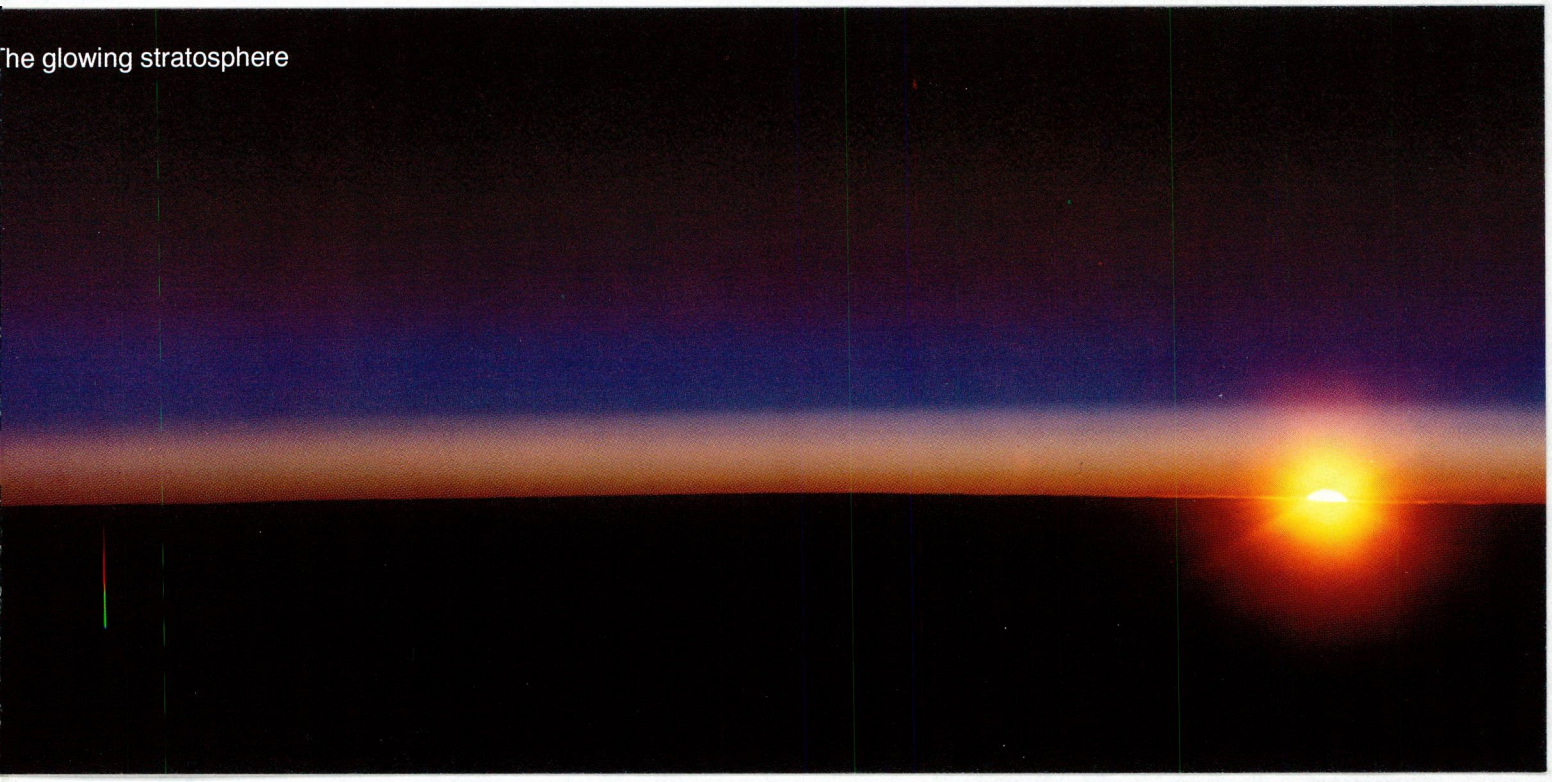

After the photographs from which the data reported here had been taken, the above picture was obtained at a solar depression angle equal to 5.7°.